Applied Science, Computing and Energy, 2026, 4(2), 217-232

Thermal Conductivity Behavior of Zig-Zag Single-Walled (7,0) Carbon Nanotube Using the Nikiforov-Uvarov Method

Otete Ikechukwu

Received: 17 November 2025/Accepted: 12 March 2026 /Published: 30 March 2026

Abstract: *The structural parameters of carbon nanotubes significantly influence thermal transport properties. In this study, the thermal behaviour of a semiconducting zig-zag single-walled (7,0) carbon nanotube was investigated using the Nikiforov–Uvarov (NU) analytical approach. Thermal conductivity was evaluated as a function of temperature, nanotube length, and diameter. The results showed that thermal conductivity increased from [κ_1 W m^{-1} K^{-1}] at [T_1 K] to a maximum value of [κ_2 W m^{-1} K^{-1}] at approximately [T_s K], after which it gradually decreased due to enhanced phonon scattering effects. Increasing the nanotube length from [L_1 nm] to [L_2 nm] resulted in a corresponding rise in thermal conductivity from [κ_3] to [κ_4 W m^{-1} K^{-1}], indicating improved phonon transport along longer tubes. Conversely, increasing the nanotube diameter from [D_1 nm] to [D_2 nm] reduced thermal conductivity by approximately [X%], attributed to increased phonon–boundary scattering. The observed thermal transport behavior is governed by the transition between ballistic phonon motion at lower dimensions and scattering-dominated transport at higher temperatures and larger diameters. These findings provide quantitative insight into structure-dependent thermal performance of semiconducting carbon nanotubes for nanoscale thermal management applications.*

Keywords: *Ballistic Phonon transport, Phonon Scattering, Thermal Conductivity, Nikiforov-Uvarov method.*

Otete Ikechukwu
Department of Physics, Federal University, Otuoke, Bayelsa State, Nigeria
Email: oteteii@fuotuoke.edu.ng
https://orcid.org/0000-0002-9150-6511

1.0 Introduction

Carbon nanotubes (CNTs) have attracted significant research interest as potential alternatives to silicon-based transistors, whose performance is increasingly limited by power consumption, heat dissipation, and current leakage associated with device miniaturization.

(Anjum, 2008; Novoselov *et al*, 2004). Mechanically, CNTs are among the strongest known materials and exhibit exceptionally high elastic modulus.

Their nanoscale dimensions and large surface area enable the attachment and assembly of nanoparticles on their surfaces. Consequently, their electrical, magnetic, and physical properties can be tuned through functionalization of either the internal cavities or external surfaces with inorganic nanoparticles (NPs) (Ado *et al*, 2008; Kim & Rina, 2011).

Efficient thermal transport is essential for the optimal performance and reliability of micro- and nano-electromechanical systems. Also, through the use of thermoelectric (TE) material and thermal interface materials (TIMs), processes are being developed to recover waste heat/conserve energy and ensure improved energy efficiency through an adequate thermal management system. However, this range of materials developed have their shortcomings in terms of their mechanical and thermal properties or too expensive and toxic to be used commercially. The exceptionally high thermal conductivity of carbon nanotubes, reported to reach values as high as 6000 W m^{-1} K^{-1}, makes them promising candidates for thermal interface materials used in heat management applications (Jianwei *et al*, 2000; Raihana & Abdul, 2019; Bogumila and David, 2019).

The mechanism of thermal transport in semiconducting zig-zag CNTs is mainly through phonons. Understanding phonon-mediated heat transport is therefore essential for predicting thermal behavior in semiconducting CNTs structures. Thermal transport through electrons is minimal because of the existence of a bandgap in the CNTs (Jin-Wu *et al*, 2010). The phonons can move with high velocity through a long path with little or no scattering because of the sp^2 hybridized c-c bonds and the low defect density. This phenomenon accounts for the high thermal conductivity of carbon nanotubes. Phonon transport corresponds to quantized lattice vibrations propagating along the carbon framework. The various vibrational modes that participate in thermal transport are the longitudinal acoustic (LA) mode, which is noticeable along the tubular axis, and the transverse acoustic (TA) mode, which is observed perpendicular to the tube axis. The others are the twisting acoustic (TW) mode; the vibrations are rotational along the tube axis, the radial breathing mode (RBM) and optical phonon modes. The longitudinal acoustic phonon mode is the outstanding one that contributes the most in thermal transport (Jungkyu, 2023).

Carbon nanotubes are cylindrical nanostructures formed by rolling graphene sheets into seamless tubes and are classified into single-walled carbon nanotubes (SWCNTs) and multi-walled carbon nanotubes (MWCNTs) (Hossein *et al*, 2020). Single-walled carbon nanotubes can be regarded as metallic or semiconducting in behavior based on their stacking or arrangement of the carbon atoms or their structural features and chirality (Phaedon *et al*, 2003; Francis, 2023).

Carbon nanotubes continue to receive extensive research attention due to their exceptional tensile strength, superior electrical properties, and remarkably high thermal conductivity which are unparalleled when compared with other conventional materials. (Sonia & Nazmul, 2018). Thus, making them find usefulness in the field of electronics/opto-electronics nanotechnology, energy and material science.

Although the thermal properties of both bulk and individual carbon nanotubes can be affected by some factors, which include the chirality, the tube length and diameters, the porosity, especially for the bulk CNTs arrays and defects (Qiang & Yonghua, 2014).

Despite extensive experimental and theoretical investigations into thermal transport in carbon nanotubes, many existing studies rely primarily on numerical simulations or empirical models. Analytical treatments capable of explicitly linking quantum mechanical energy states to thermodynamic transport properties remain limited, particularly for specific chiral semiconducting nanotubes such as the zig-zag (7,0) configuration under external field effects. Consequently, a rigorous analytical framework for evaluating thermal conductivity in such systems is still lacking.

Therefore, this study aims to analytically investigate the thermal conductivity behavior of a semiconducting zig-zag single-walled (7,0) carbon nanotube using the Nikiforov–Uvarov (NU) method.

The significance of this study lies in providing an analytical framework that connects quantum mechanical energy solutions with macroscopic thermal transport behavior, thereby contributing to improved theoretical understanding and potential design optimization of nanoscale thermal management materials.

In the quest to search for a material whose device applications can be miniaturized and as well perform optimally as an interconnect in integrated electronics, it becomes imperative to study the thermal conductivity behavior of zig-zag single-walled (7,0) carbon nanotube with Nikiforov-Uvarov (NU) method. Zig-zag single-walled (7,0) carbon nanotube is a

semiconductor based on the chirality rule of $n - m \neq 3k$ where k is an integer and n is not a multiple of 3 (Jian-Min *et al*, 2010). It has a lattice (unit-cell length) and diameter of approximately 0.426nm and 0.55nm respectively (Saito *et al*, 1998). The carbon atoms per unit cell is 28 atoms (Yusuke *et al*, 2020). As reported by Takashi and Susumu, (2004), the geometry-optimized local density approximation band gap value is approximately 0.2eV. In this work, the Schrödinger wave equation incorporating the Deng–Fan–Hulthén potential, magnetic field effects, and Aharonov–Bohm (AB) flux is solved analytically using the Nikiforov–Uvarov method to obtain the energy eigenvalue spectrum and corresponding wave functions.

With the energy equation, the partition function is calculated, and thereafter, the thermodynamic property of thermal conductivity is evaluated with the Maple software.

This paper is organized as follows; in section 2, the Hamiltonian of a charged particle interacting with magnetic field B and Ahanorov-Bohm (AB) flux where the Schrödinger wave equation is solved with Nikiforov-Uvarov (NU) method analytically is considered. The calculation of the partition function used to evaluate the thermodynamic property of conductivity is done in section 3. The results and discussion are done in section 4. The conclusion is done in the last section followed by the references.

2.0 Theoretical Model and Mathematical Formulation

In a cylindrical coordinate system, the quantum Hamiltonian describing a charged particle confined in a Deng–Fan–Hulthén potential under the combined influence of an external magnetic field B and Ahanorov-Bohm (AB) flux as shown in equation (1):

$$\frac{1}{2\mu}(i\hbar\vec{\nabla} - \frac{q}{c})^2 + D_e\left(1 - \frac{\eta}{(e^{\vartheta r}-1)}\right)^2 - \frac{V_o e^{\vartheta r}}{(1- e^{-\vartheta r})} = E_{(n,m)}\psi_{(\rho,\varphi,z)} \quad (1)$$

where $\eta = e^{\vartheta r_e}$ -1, D_e represents the dissociation energy, r_e stands for the molecular bond length, r is the internuclear distance, η, is the range of the potential well and V_o stands for the potential strength (Otete, 2026).

The parameter, μ represents the effective mass for the CNT, single-walled carbon nanotube. $\vec{A} = \vec{A}_1 + \vec{A}_2$ is the vector potential with a combination of $\vec{A}_1$ and $\vec{A}_2$. The Coulomb gauge is taken to be $\nabla\times\vec{A}_1 = \vec{B}$ and $\nabla\times\vec{A}_2 = 0$. $\vec{B}$ is the applied magnetic field along the z-direction. The magnetic flux Φ_{AB} is created by the solenoid. Therefore, in the cylindrical coordinate system, the vector potential with the azimuthal components is written as (Otete, 2026

$$\vec{A}_1 = \frac{\vec{B}e^{-\vartheta r}}{(1-e^{-\vartheta r})}, \vec{A}_2 = \frac{\Phi_{AB}}{2\pi r}\hat{\Phi}. \text{ So, } \vec{A} = \left(0, \frac{\vec{B}e^{-\vartheta r}}{(1-e^{-\vartheta r})} + \frac{\Phi_{AB}}{2\pi r}, 0\right) \quad (2)$$

The qualitative behavior of the Deng–Fan–Hulthén potential used in this study is illustrated in Fig. 1.

In the cylindrical coordinates our wave function is taken as:

$$\psi_{(r,\varphi)} = \frac{1}{\sqrt{2\pi}} e^{im\varphi}\ U_{nm,}(r)\ m = 0, \pm 1, \pm 2 \ldots \quad (3)$$

where m represents the magnetic quantum number. By inserting our potential, vector potential and the wave function into Eq. (1), a second order differential equation of the form will be obtained:

$\frac{d^2U_{nm}(r)}{dr^2} + \frac{2\mu}{\hbar^2}\left[E - D_e\left(1 - \frac{\eta}{(e^{\vartheta r}-1)}\right)^2 + \frac{V_o e^{-\vartheta r}}{(1-e^{-\vartheta r})} - \frac{2\hbar m e\vartheta \vec{B} e^{-\vartheta r}}{c(1-e^{-\vartheta r})} - \frac{e^2\vec{B}e^{-2\vartheta r}}{c^2(1-e^{-\vartheta r})^2} - \frac{e^2\vec{B}\Phi_{AB}e^{-\vartheta r}}{c^2(1-e^{-\vartheta r})^2 2\pi r} - \frac{((m+\xi)-\frac{1}{4})}{r^2}\right]U_{nm}(r) = 0$ (4)

Since the resulting equation contains both exponential and centrifugal terms, the improved Greene–Aldrich approximation is employed to treat the centrifugal term as equation 5 (Otete, 2026).

$\frac{1}{r^2} \approx \vartheta^2\left[d_o + \frac{e^{-\vartheta r}}{(1-e^{-\vartheta r})^2}\right]$ (5)

By inserting Eq. (5) into Eq. (4) we have

$\frac{d^2U_{nm}(r)}{dr^2} + \left[\frac{2\mu E}{\hbar^2} - \frac{2\mu D_e}{\hbar^2} + \frac{4\mu D_e\eta e^{-\vartheta r}}{\hbar^2(1-e^{-\vartheta r})} \frac{2D_e\eta^2 e^{-2\vartheta r}}{\hbar^2(1-e^{-\vartheta r})^2} + \frac{2V_o e^{-\vartheta r}}{\hbar^2(1-e^{-\vartheta r})} - \frac{2m\mathfrak{n}\vartheta\vec{B}e^{-\vartheta r}}{\hbar^2(1-e^{-\vartheta r})^2} - \frac{\mathfrak{n}^2\overrightarrow{B^2}e^{-2\vartheta r}}{\hbar^2(1-e^{-\vartheta r})^2} - \frac{\mathfrak{n}^2\vartheta\vec{B}\Phi_{AB}e^{-\vartheta r}}{\hbar^2(1-e^{-\vartheta r})^2\pi} - ((m+\xi)-\frac{1}{4})\vartheta^2\left(d_o + \frac{e^{-\vartheta r}}{(1-e^{-\vartheta r})^2}\right) \right] U_{nm}(r) = 0$ (6)

where $\mathfrak{n} = \frac{e}{c}$, $\Phi_o = \frac{\hbar c}{e}$, $\xi = \frac{\Phi_{AB}}{\Phi_o}$ and $\eta = e^{\vartheta r} - 1$, c is the speed of light.

To simplify the analytical solution using the Nikiforov–Uvarov method, the coordinate transformation of equation (7) is done.

$\mathfrak{s} = e^{-\vartheta r}$ (7)

Differentiation with respect to the transformed variable yields:

$\frac{d^2}{d\mathfrak{s}^2} = \frac{\vartheta^2\mathfrak{s}^2 d^2}{d\mathfrak{s}^2} + \frac{\vartheta^2\mathfrak{s}d}{d\mathfrak{s}}$ (8)

Substituting Eq. (8) into Eq. (6) and dividing through by $\mathfrak{\lambda}^2\mathfrak{z}^2$ the result will be:

$\frac{d^2U_{nm}}{d\mathfrak{z}^2} + \frac{1}{\mathfrak{z}}\frac{dU_{nm}}{d\mathfrak{z}} + \frac{1}{\mathfrak{z}^2}\left[\frac{2\mu E}{\hbar^2\vartheta^2} - \frac{2\mu D_e}{\hbar^2\vartheta^2} + \frac{4\mu D_e\eta\mathfrak{z}}{\hbar^2\vartheta^2(1-\mathfrak{z})} - \frac{2\mu D_e\eta^2\mathfrak{z}^2}{\hbar^2\vartheta^2(1-\mathfrak{z})^2} + \frac{2\mu V_o\mathfrak{z}}{\hbar^2\vartheta^2(1-\mathfrak{z})} - \frac{2m\eta\vec{B}\mathfrak{z}}{\hbar\vartheta(1-\mathfrak{z})^2} - \frac{\mathfrak{n}^2\vec{B}^2\mathfrak{z}^2}{\hbar^2\vartheta(1-\mathfrak{z})^2} - \frac{\mathfrak{n}^2\vec{B}\Phi_{AB}\mathfrak{z}}{\hbar^2\vartheta(-\mathfrak{z})^2\pi} - \left((m+\zeta)^2 - \frac{1}{4}\right)\left(d_o + \frac{\mathfrak{z}}{(1-\mathfrak{z})^2}\right)\right] U_{nm}(r) = 0$ (9)

For mathematical convenience and compact representation, the following dimensionless parameters are introduced:

$-\varepsilon = \frac{2\mu(E_{nm}-D_e)}{\hbar^2\vartheta^2}$, $\Upsilon_1 = \frac{4\mu D_e\mathfrak{y}}{\hbar^2\vartheta^2}$, $\Upsilon_2 = \frac{2\mu D_e\mathfrak{y}^2}{\hbar^2\vartheta^2}$, $\mathfrak{b} = \frac{2\mu V_o}{\hbar^2\vartheta^2}$, $\varkappa = \frac{2m\eta\vec{B}}{\hbar\vartheta}$, $\chi_1 = \frac{\mathfrak{n}^2\vec{B}^2}{\hbar^2\vartheta^2}$, $\chi_2 = \frac{\mathfrak{n}^2\vec{B}\Phi_{AB}}{\hbar^2\vartheta^2\pi}$, $\Delta = \left((m+\xi)^2 - \frac{1}{4}\right)$ (10)

Equation (9) can be rewritten with respect to these dimensionless symbols as:

$\frac{d^2U_{nm}}{d\mathfrak{z}^2} + \frac{(1-\mathfrak{z})}{\mathfrak{z}(1-\mathfrak{z})}\frac{dU_{nm}}{d\mathfrak{z}} + \frac{1}{\mathfrak{z}^2(1-\mathfrak{z})^2}\left[-\varepsilon(1-\mathfrak{z})^2 + \Upsilon_1(1-\mathfrak{z})\mathfrak{z} - \Upsilon_2(\mathfrak{z}^2) + \mathfrak{b}(1-\mathfrak{z})\mathfrak{z} - \varkappa(\mathfrak{z}) - \chi_1(\mathfrak{z}^2) - \chi_2(1-\mathfrak{z})\mathfrak{z} - \Delta d_o(1-\mathfrak{z})^2 - \Delta(\mathfrak{z})\right] U_{nm} = 0$ (11)

Equation (12) is now compared with the standard parametric form of the Nikiforov–Uvarov (NU) differential equation given by (Otete & Eleje, 2023):

$\frac{d^2U_{nm}}{d\mathfrak{z}^2} + \frac{(1-\mathfrak{z})}{\mathfrak{z}(1-\mathfrak{z})}\frac{dU_{nm}}{d\mathfrak{z}} + \frac{1}{\mathfrak{z}^2(1-\mathfrak{z})^2}\left[-(\varepsilon + \Upsilon_1 + \Upsilon_2 + \mathfrak{b} + \chi_1 - \chi_2 + \Delta d_o)\mathfrak{z}^2 + (2\varepsilon + \Upsilon_1 + \mathfrak{b} - \varkappa - \chi_2 + 2\Delta d_o - \Delta)\mathfrak{z} - (\varepsilon + \Delta d_o)\right] U_{nm} = 0$ (12)

Equation (12) is compared with the parametric form of the NU of Eq. (13) is written as (Otete & Eleje, 2023) :

$U''_{(\mathfrak{z})} + \frac{\mu_1 - \mu_2\mathfrak{z}}{\mathfrak{z}(1-\mu_3\mathfrak{z})}U'_{(\mathfrak{z})} + \left[\frac{-\zeta_1\mathfrak{z}^2 + \zeta_2\mathfrak{z} - \zeta_3}{\mathfrak{z}^2(1-\mu_3\mathfrak{z})^2}\right] R_{(\mathfrak{z})} = 0$ (13)

The energy eigen values equation according to the NU is written as (Otete & Ejere, 2025):

$\mu_2 n-(2n+1)\mu_5+ (2n+1) [\sqrt{\mu_9} + \mu_3\sqrt{\mu_8}] +n (n-1)\mu_3+\mu_7+2\mu_3\mu_8+2\sqrt{\mu_8\mu_9} = 0$ (14)

The corresponding normalized radial wavefunction is expressed as:

$U_{nm}(z) = z^{\mu_{12}}(1 - \mu_3 z)^{-\mu_{12}-\mu_{13}/\mu_3}\, p_n^{\mu_{10}-1,\left(\frac{\mu_{11}}{\mu_3}\right)-(\mu_{10}-1)}(1-2\mu_3 z)$ (15)

where the following parameters are written as

$\mu_4 = \frac{1}{2}(1-\mu_1)$ (16)

$\mu_5 = \frac{1}{2}(\mu_2 - 2\mu_3)$ (17)

$\mu_6 = \mu_5 + \zeta_1$ (18)

$\mu_7 = 2\mu_4\mu_5 - \zeta_2$ (19)

$\mu_8 = \mu^2{}_4 + \zeta_3$ (20)

$\mu_9 = \mu_3\mu_7 + \mu^2{}_3\mu_8 + \mu_6$ (21)

$\mu_{10} = \mu_1 + 2\mu_4 + 2\sqrt{\mu_8}$ (22)

$\mu_{11} = \mu_2 - 2\mu_5 + 2(\sqrt{\mu_9} + \mu_3\sqrt{\mu_8})$ (23)

$\mu_{12} = \mu_4 + \sqrt{\mu_8}$ (24)

$\mu_{13} = \mu_5 - (\sqrt{\mu_9} + \mu_3\sqrt{\mu_8})$ (25)

Upon comparing equation 12 with the parametric form of the NU of Eq. (13) the corresponding parameters are identified as:

$\mu_1 = \mu_2 = \mu_3 = 1$ (26)

$\zeta_1 = \varepsilon + \Upsilon_1 + \Upsilon_2 + \beta + \chi_1 - \chi_2 + \Delta d_o$ (27)

$\zeta_2 = 2\varepsilon + \Upsilon_1 + \beta - \varkappa - \chi_2 + 2\Delta d_o - \Delta$ (28)

$\zeta_3 = \varepsilon + \Delta d_o$ (29)

From Eqs. (16-21) we obtain

$\mu_4 = \frac{1}{2}(1-\mu_1) = 0, \mu_5 = \frac{1}{2}(\mu_2 - 2\mu_3) = -\frac{1}{2}, \mu_6 = \mu_5^2 + \zeta_1 = \frac{1}{4} + \varepsilon + \Upsilon_1 + \Upsilon_2 + \beta + \chi_1 - \chi_2 + \Delta d_o$ (30)

$\mu_7 = 2\mu_4\mu_5 - \zeta_2 = -(2\varepsilon + \mu_1 + \beta - \varkappa - \chi_2 + 2\Delta d_o - \Delta)$ (31)

$\mu_8 = \mu_4^2 + \zeta_3 = \varepsilon + \Delta d_o$ (32)

$\mu_9 = \mu_3\mu_7 + \mu_3^2\mu_8 + \mu_6 = \frac{1}{4} + \varkappa + \Delta + \chi_1 + \Upsilon_2$ (33)

Recall that in Eq. (10), $-\varepsilon = \frac{2\mu(E_{nm}-D_e)}{\hbar^2\vartheta^2}$ (34)

So, substituting Eqs. (30-33) into Eq. (14) and after straightforward algebraic simplification, the energy eigenvalue equation of the Deng-Fan-Hulthen potential is obtained as:

$$E_{nm} = -\frac{\hbar^2\vartheta^2}{2\mu}\left[\left(\frac{(\alpha-\lambda)}{2(\gamma+\sqrt{\alpha})} - \frac{(\gamma+\sqrt{\alpha})}{2}\right)^2 - \Delta d_o + D_e\right] \quad (35)$$

Where

$$\alpha = \frac{1}{4} + \varkappa + \Delta + \chi_1 + \Upsilon_2,\ \lambda = -\Upsilon_1 - \mathfrak{b} + \varkappa + \chi_2 + \Delta, \gamma = n + \frac{1}{2} \tag{36}$$

Thus, Eq. (36) can be re-written in terms of the dimensionless symbols of Eq. (10) as:

$$\alpha = \frac{1}{4} + \frac{2m\eta\vec{B}}{\hbar\vartheta} + (m+\zeta)^2 - \frac{1}{4} + \frac{\mathfrak{n}^2\vec{B}^2}{\hbar^2\vartheta^2} + \frac{2\mu D_e\mathfrak{y}^2}{\hbar^2\vartheta^2} \tag{37}$$

$$\lambda = -\frac{4\mu D_e\mathfrak{y}}{\hbar^2\vartheta^2} - \frac{2\mu V_o}{\hbar^2\vartheta^2} + \frac{2m\eta\vec{B}}{\hbar\vartheta} + \frac{\mathfrak{n}^2\vec{B}\Phi_{AB}}{\hbar^2\vartheta\pi} + (m+\zeta)^2 - \frac{1}{4} \tag{38}$$

From Eqs. (22-25) we determine

$$\mathfrak{M}_{10} = \mathfrak{M}_1 + 2\mathfrak{M}_4 + 2\sqrt{\mathfrak{M}_8} = 1 + 2\sqrt{\varepsilon + \Delta d_0} \tag{39}$$

$$\mathfrak{M}_{11} = \mathfrak{M}_2 - 2\mathfrak{M}_5 + 2(\sqrt{\mathfrak{M}_9 + \mathfrak{M}_3\mathfrak{M}_8} = 2 + 2\left(\sqrt{\frac{1}{4} + \varkappa + \Delta + \chi_1 + \Upsilon_2 + \varepsilon + \Delta d_0}\right) \tag{40}$$

$$\mathfrak{M}_{12} = \mathfrak{M}_4 + \sqrt{\mathfrak{M}_8} = \sqrt{\varepsilon + \Delta d_0} \tag{41}$$

$$\mathfrak{M}_{13} = \mathfrak{M}_5 - (\sqrt{\mathfrak{M}_9} + \mathfrak{M}_3\sqrt{\mathfrak{M}_8}) = -\frac{1}{2} - \left(\sqrt{\frac{1}{4} + \varkappa + \Delta + \chi_1 + \Upsilon_2} + \sqrt{\varepsilon + \Delta d_0}\right) \tag{42}$$

Substituting Eqs. (39-42) into Eq. (15) the wave function written in Eq. (43) is obtained.

$$U_{nm}(\mathrm{z}) = \mathrm{z}^{\sqrt{\varepsilon+\Delta d_0}}(1-\mathrm{z})^{\frac{1}{2}+\sqrt{\frac{1}{4}+\varkappa+\Delta+\chi_1+\Upsilon_2}} P_n^{2\sqrt{\varepsilon+\Delta d_0},2\sqrt{\frac{1}{4}+\varkappa+\Delta+\chi_1+\Upsilon_2}}(1-2\mathrm{z}) \tag{43}$$

3.0 The Partition Function and the Thermodynamic Properties of Carbon Nanotube

Thermal conductivity is one aspect of the thermodynamic properties of nanotube that can be determined. For this property to be calculated the partition function which is temperature dependent, is first evaluated. At a given temperature, when a direct summation is performed over all possible energy levels, the partition function can be obtained. The partition function is written as (Otete *et al*, 2024):

$$Z(\beta) = \sum_{n}^{v_{max}} e^{-\beta E_{n,m}} \tag{44}$$

where $\beta = (KT)^{-1}$ with K as the Boltzmann constant, T, the temperature E_{nm} is the energy of the nth bound state where $n = 0, 1, 2, 3 \ldots, v_{max}$.

The energy eigenvalue of equation (35) can be rewritten as:

$$E_{nm} = -\hbar^2\vartheta^2\left(\frac{N_1-(n+\alpha)^2}{2(n+\alpha)}\right)^2 + N_2 \tag{45}$$

Where

$$K_1 = \frac{1}{4} + \frac{2m\eta\vec{B}}{\hbar\vartheta} + (m+\zeta)^2 - \frac{1}{4} + \frac{\mathfrak{n}^2\vec{B}^2}{\hbar^2\vartheta^2} + \frac{2\mu D_e\mathfrak{y}^2}{\hbar^2\vartheta^2} + \frac{4\mu D_e\mathfrak{y}}{\hbar^2\vartheta^2} - \frac{2\mu V_o}{\hbar^2\vartheta^2} + \frac{2m\eta\vec{B}}{\hbar\vartheta} + \frac{\mathfrak{n}^2\vec{B}\Phi_{AB}}{\hbar^2\vartheta\pi} + (m+\zeta)^2 - \frac{1}{4} \tag{46}$$

$$K_2 = \left((m+\xi)^2 - \frac{1}{4}\right) d_o\left(\frac{\hbar^2\mathfrak{\lambda}^2}{2\boldsymbol{\mu}}\right) + D_e \tag{47}$$

Therefore, equation (44) can be recast as:

$$Z(\beta) = \sum_{n}^{v_{max}} e^{-\beta\left[-\frac{\hbar^2\vartheta^2}{2\mu}\left(\frac{N_1-(n+\alpha)^2}{2(n+\alpha)}\right)^2 + K_2\right]} \tag{48}$$

In the classical limit, the summation of equation (48) is replaced by an integral therefore we have

$$Z_{(\beta)} = \int_0^{\upsilon} e^{\left(Pl^2\beta + \frac{G\beta}{l^2} + M\beta\right)} dl, l = n + \alpha \quad (49)$$

Where

$$P = \frac{\hbar^2\vartheta^2}{8\mu}, G = -\frac{\hbar^2\vartheta^2 K_1^2}{8\mu}, M = -\left(\frac{\hbar^2\vartheta^2 N_1}{4\mu} + K_2\right) \quad (50)$$

The Maple software is used to evaluate equation (49) to obtain the partition function of the system as

$$\frac{1}{2} e^{P.\beta.l^2 + M.\beta\sqrt{G.\beta}} \left(\frac{2.v.e^{\frac{G.\beta}{v^2}}}{\sqrt{G.\beta}} - \frac{2\sqrt{G.\beta}\ \sqrt{\pi}\ erfi\left(\frac{G.\beta}{v}\right)}{\sqrt{G.\beta}} - 2\sqrt{\pi} \right) \quad (51)$$

Where erfi(k) denotes the imaginary error function (Edet *et al*, 2020) define as

$$\text{erfi}(k) = ierf(k) = \frac{2}{\sqrt{\pi}} \int_0^k e^{t^2} dt \quad (52)$$

In Maple software, this error function is used for various numerical calculations.

With the partition function of the system known, the thermal conductivity K, which is a function of heat capacity, phonon group velocity and the free mean path can be. The thermal conductivity of CNTs can be written as (Michael & Jang-Yu, 2009):

$$K = \frac{1}{3} \rho c v^2 \tau_s \quad (53)$$

Here, c, v, and τstands for specific heat per unit volume, group velocity and relaxation time or free mean path of a given phonon state, respectively (Bounphanh, 2011). The specific heat capacity is given by the relation (Khordad & Rastegar, 2017):

$$\text{Specific heat } C_v = \frac{\partial U}{\partial T} = k_B \beta^2 \frac{\partial^2 lnZ}{\partial \beta^2} \quad (54)$$

So, the thermal conductivity can be writen as:

Thermal conductivity

$$K = \frac{1}{3} \rho v^2 \tau_s k_B \beta^2 \frac{\partial^2 lnZ}{\partial \beta^2} \quad (55)$$

Below is the graphical behavior of Deng-Fan-Hulthen potential.

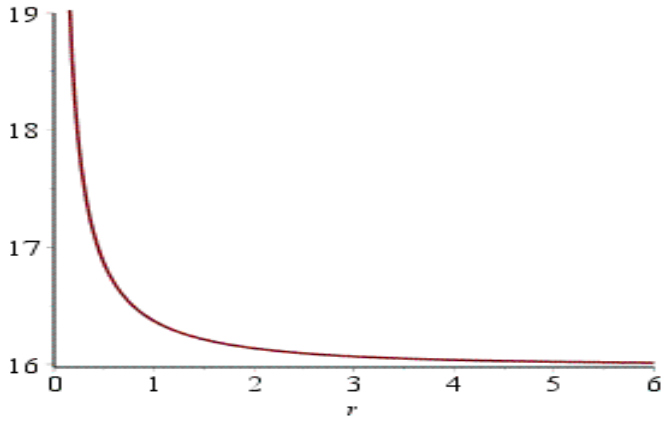

Fig. 1 Deng-Fan-Hulthen Potential graphical behavior

We present the graphical plots of the thermal conductivity with temperature variation and bond length in Figs. 2, 3 and 4.

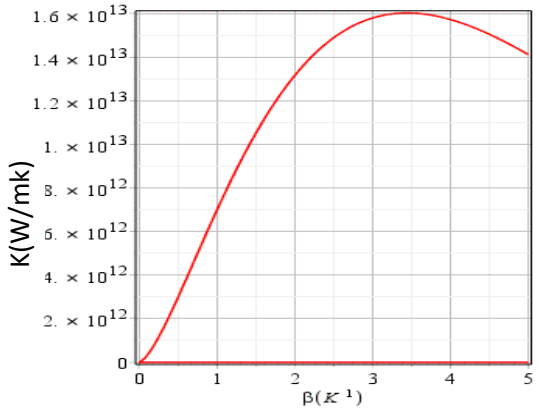

Fig. 2: Plot of thermal conductivity versus temperature

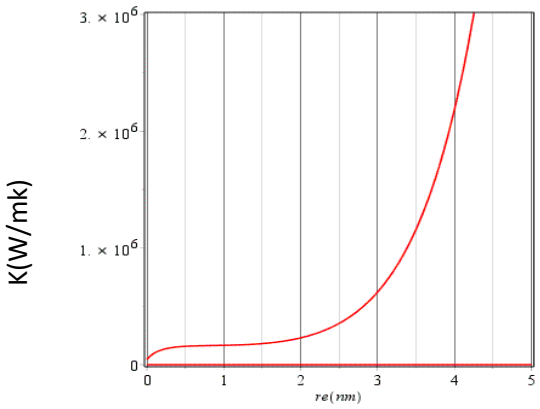

Fig. 3 Plot of thermal conductivity versus tube length

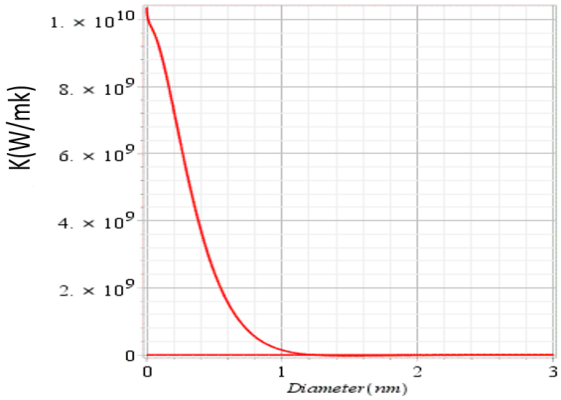

Fig 4: Plot of thermal conductivity versus tube diameter

Fig. 2 depicts the variation of thermal conductivity with temperature.

4.0 Results and Discussion

It is observed that thermal conductivity increases with increasing temperature. However, beyond a critical temperature, the thermal conductivity reaches a maximum and subsequently decreases. This behavior can be attributed to phonon transport mechanism. At lower temperatures, ballistic phonon transport dominates, leading to an increase in thermal conductivity. As temperature increases further, enhanced phonon–phonon scattering reduces heat transport efficiency, resulting in decreased thermal conductivity (Zahra *et al*., 2024). Fig. 3 shows the variation of thermal conductivity with nanotube length. Thermal conductivity increases significantly with increasing nanotube length.

This trend is attributed to enhanced ballistic transport arising from an increase in phonon mean free path with nanotube length.

Fig. 4 illustrates that thermal conductivity is inversely proportional to nanotube diameter.

As the tube diameter increases, the thermal conductivity tends to decrease. With less thermal transport, the thermal conductivity decreases as the diameter increases (Vikas *et al*, 2018).

5.0 Conclusion

The thermal conductivity behavior of a zig-zag single-walled (7,0) carbon nanotube was analytically investigated using the Nikiforov–Uvarov (NU) method through the solution of the Schrödinger wave equation. The derived energy eigenvalues enabled the calculation of the partition function, which was subsequently employed to evaluate thermal conductivity as a thermodynamic property dependent on temperature, nanotube length, and diameter.

The results show that thermal conductivity increases with temperature at lower regimes due to dominant ballistic phonon transport, reaching a maximum value before decreasing at higher temperatures as a result of enhanced phonon–phonon scattering. Furthermore, thermal conductivity was found to increase with nanotube length, attributed to an extended phonon mean free path that promotes efficient heat transport. In contrast, an increase in nanotube diameter led to a reduction in thermal conductivity, which is associated with increased phonon scattering and redistribution of vibrational modes.

These findings highlight the strong dependence of thermal transport properties on structural parameters of carbon nanotubes and reinforce their potential application in nanoscale thermal management systems. The high thermal conductivity exhibited by the (7,0) single-walled carbon nanotube suggests its suitability for integration into CNT-based heat dissipation and thermal interface materials for advanced electronic and nanoelectronic devices.

6.0 References

Ado, J., Gene, D., & Mildred, S. D. (Eds.). (2008). *Carbon nanotubes: Advanced topics in the synthesis, structure, properties and applications*. Springer-Verlag.

Anjum, F. (2008). *Spintronics: Fundamentals and applications* (EE453 Project Report). [Unpublished manuscript or Technical Report].

Bogumila, K., & Dawid, J. (2019). Thermal conductivity of carbon nanotube networks: A review. *Journal of Materials Science*, *54*(10), 7397–7427. https://doi.org/10.1007/s10853-019-03317-x

Bounphanh, T. (2011). *Thermal and mechanical studies of carbon nanotube-polymer composites synthesized at high pressure and high temperature* [Doctoral thesis, University of Umea]. DiVA Portal.

Edet, C.O., Okoi, P. O., Yusuf, A. S., & Ushie, P. O. (2020). Bound state solutions of the generalized shifted Hulthen potential. *Indian Journal of Physics*, *95*(3), 543–551. https://doi.org/10.1007/s12648-019-01650-0

Francis, A. (2023). Thermoresistivity of carbon nanostructures and their polymeric nanocomposites. *Advanced Materials Interfaces*, *10*(31), Article 2300218. https://doi.org/10.1002/admi.202300218

Hosseini, K. M., Mamad, R. M., & Amir, R. (2020). Application of carbon nanotubes (CNT) on the computer science and electrical engineering: A review. *International Journal of Reconfigurable and Embedded Systems (IJRES)*, *9*(1), 61–82. http://doi.org/10.11591/ijres.v9.i1.pp61-82

Jian-Min, Z., Rui-Li, L., & Ke-Wei, X. (2010). Effect of uniaxial strain on the band gap of zig-zag carbon nanotubes. *Physica B: Condensed Matter*, *405*(5), 1329–1334. https://doi.org/10.1016/j.physb.2009.11.082

Jianwei, C., Tahir, C., & Williams, A. G. (2000). Thermal conductivity of carbon nanotubes. *Nanotechnology*, *11*(2), 65–69. https://doi.org/10.1088/0957-4484/11/2/305

Jian-Wu, J., Jiang-Sheng, W., & Baowen, L. (2010). *A nonequilibrium Green's function study of thermoelectric properties in single-walled carbon nanotubes*. arXiv. https://doi.org/10.48550/arXiv.1012.1081

Jungkyu, P. (2023). Thermal transport study in a strained carbon nanotube and graphene junction using phonon wavepacket analysis. *C — Journal of Carbon Research*, *9*(1), Article 21. https://doi.org/10.3390/c9010021

Khordad, R., & Rastegar, S. H. R. (2017). Thermodynamic properties of a double ring-shaped quantum at low and high temperatures. *Journal of Low Temperature Physics*, *188*, 141–154. https://doi.org/10.1007/s10909-017-1831-x

Kim, I. I. T., & Rina, T. (2011). Magnetic carbon nanotubes: Synthesis, characterization, and anisotropic electrical properties. In J. M. Marulanda (Ed.), *Electronic properties of carbon nanotubes* (pp. 317–334). InTech. https://doi.org/10.5772/15392

Michael, C. H. W., & Jang-Yu, H. (2009). Thermal conductivity of carbon nanotubes with quantum correction via heat capacity. *Nanotechnology*, *20*(14), Article 145401. https://doi.org/10.1088/09574484/20/14/145401

Novoselov, K. S., Geim, A. K., Morozov, S. V., Jiang, D., Zhang, Y., Dubonos, S. V., Grigorieva, I. V., & Firsov, A. A. (2004). Electric field effect in atomically thin carbon films. *Science*, *306*(5696), 666–669. https://doi.org/10.1126/science.1102896

Otete, I. (2026). Analytical study of the thermoresistivity behavior of single-walled (10,0) zig-zag carbon nanotube using the Deng-Fan-Hulthen potential model. *Communication in Physical Sciences*, *13*(2), 212–222. https://dx.doi.org/10.4314/cps.vi3i2.4

Otete, I., & Eleje, C. B. (2023). Magnetic field effect on the energy spectra of InP quantum dot in D-dimensions with Hulthen-Yukawa potential. *Asian Research Journal of Current Science*, *5*(1), 20–27.

Otete, I., & Ejere, A. I. (2025). The D-dimensional analysis of magnetic field, potential depth and screening parameter impact on the energy spectra of lead selenide. *Benin Journal of Physical Sciences*, *2*(2), 184–193.

Otete, I., Enaroseha, O. O. E., Okunzuwa, S. I., & Ejere, A. I. I. (2024). Spectra and thermodynamic properties of zig-zag single-walled carbon nanotubes with Deng-Fan-Hulthen potential. *Ukrainian Journal of Physics*, *69*(10), 719. https://doi.org/10.15407/ujpe69.10.719

Phaedon, A., Joerg, A., Richard, M., & Shalom, W. J. (2003). Carbon nanotube electronics. *Proceedings of the IEEE*,

91(11), 1772–1784. https://doi.org/n10.1109/JPROC.2003.818324

Qiang, C., & Yonghua, H. (2014). A practical dimensionless equation for the thermal conductivity of carbon nanotubes and CNT arrays. *AIP Advances*, *4*(5), Article 057115. https://doi.org/10.1063/1.4878785

Raihana, B., & Abdul, R. M. (2019). Effect of carbon nanotubes as thermal interface materials on thermal conductivity using electrophoretic deposition. *Journal of Physical Science*, *30*(Supp. 1), 149–158. https://doi.org/10.21315/jps2019.30.S1.9

Saito, R., Dresselhaus, G., & Dresselhaus, M. S. (1998). *Physical properties of carbon nanotubes*. World Scientific Publishing. https://doi.org/10.1142/p080

Sonia, K., & Nazmul, I. (2018). Carbon nanotubes-properties and applications. *Organic & Medicinal Chemistry International Journal*, *7*(1), Article 555705. https://doi.org/10.19080/OMCIJ.2018.07.555705

Takashi, M., & Susumu, S. (2004). Quasiparticle band structure of carbon nanotubes. *Transactions of the Materials Research Society of Japan*, *29*(2), 553–557.

Varshney, V., Lee, J., Brown, J., Farmer, B. L., Voevodin, A. A., & Roy, A. K. (2018). Effect of length, diameter, chirality, deformation and strain on contact thermal conductance between single-wall carbon nanotubes. *Frontiers in Materials*, *5*, Article 17. https://doi.org/10.3389/fmats.2018.00017

Yusuke, A., Motoaki, H., & Shuichi, M. (2020). Anomalous dielectric response in insulators with the Zak phase. *Physical Review B*, *102*(4), Article 041112. https://doi.org/10.1103/PhysRevB.102.041112

Zahra, A. T., Aamir, S., Alina, M., Jamoliddin, R., Quratul, A. A., Asif, K., & Guogang, R. (2024). Structural and thermal analyses in semiconducting and metallic zig-zag single-walled carbon nanotubes using molecular dynamics simulations. *PLOS ONE*, *19*(2), Article e0296916. https://doi.org/10.1371/journal.pone.0296916

Declaration

Consent for publication

Not Applicable

Availability of data and materials

The publisher has the right to make the data public

Conflict of Interest

The authors declared no conflict of interest

Ethical Considerations

Not applicable

Competing interest

The authors report no conflict or competing interest

Funding

The author declared no source of funding

Authors' Contributions

All aspects of the work were carried out by the author